ACS APPLIED MATERIALS & INTERFACES

Research Article

www.acsami.org

Effect of Chain Length on the Sensing of Volatile Organic Compounds by means of Silicon Nanowires

Bin Wang and Hossam Haick*

The Department of Chemical Engineering and Russell Berrie Nanotechnology Institute, Technion–Israel Institute of Technology, Haifa 3200003, Israel

ABSTRACT: Molecularly modified silicon nanowire field effect transistors (SiNW FETs) are starting to appear as promising devices for sensing various volatile organic compounds (VOCs). Understanding the connection between the molecular layer structure attached to the SiNWs and VOCs is essential for the design of high performance sensors. Here, we explore the chain length influence of molecular layers on the sensing performance to polar and nonpolar VOCs. SiNW FETs were functionalized with molecular layers that have similar end (methyl) group and amide bridge bond, but differ in their alkyl chain lengths. The resulting devices were then exposed to polar and nonpolar VOCs in various concentrations. Our results showed that the sensing response to changing the threshold voltage (ΔV_{th}) and changing the relative hole mobility ($\Delta\mu_h/\mu_{h\text{-}a}$) have a proportional relationship to the VOC concentration. On exposure to a specific VOC concentration, ΔV_{th} response increased with the chain length of the molecular modification. In contrast, $\Delta\mu_h/\mu_{h\text{-}a}$ did not exhibit any obvious reliance on the chain length of the molecular layer. Analysis of the responses with an electrostatic-based model suggests that the sensor response in ΔV_{th} is dependent on the VOC concentration, VOC vapor pressure, VOC–molecular layer binding energy, and VOC adsorption-induced dipole moment changes of molecular layer.

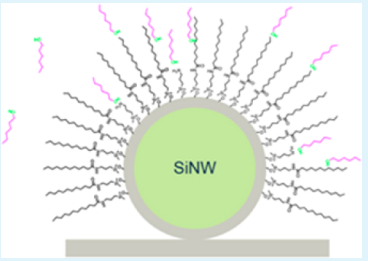

KEYWORDS: *silicon nanowire, field effect transistor, vapor sensor, dipole, volatile organic compound*

INTRODUCTION

Sensing volatile organic compounds (VOCs) is of utmost importance to environmental monitoring and human health.[1−15] The VOCs are mainly linked with emissions from transportation, industrial processes, and use of organic solvents.[1] Even at relatively low concentration, some toxic and carcinogenic VOCs released in the atmosphere may be dangerous to human health.[1] On the other hand, VOCs obtained in breath samples have been associated with certain diseases, so they have been used as biomarkers for disease diagnoses by breath analysis.[2−4,16−23] To fulfill the potential of detecting these real world VOCs, it is essential to develop high-performance gas sensors.

Silicon nanowire (SiNW) field-effect transistor (FET)-based sensors have been successfully applied in sensing chemical and biological species in gas and liquid phases.[5−8,23−36] Using SiNW FETs provides distinct advantages over other sensing strategies, because of (i) the ability to fine-tune the sensing response by controlling gate voltages; (ii) the ability to provide more features (parameters) to evaluate sensor sensitivity by one test; (iii) the low power consumption and the extreme miniaturization of the device. Molecular engineering of the SiNW surface is a promising approach for improving the sensitivity of SiNW devices to VOCs, because it allows for controlling the stability,[37,38] (cf. also refs 39−41) tarp states,[5,6,37,42] electrical properties of SiNWs,[5−7,26,37,42−45] and hence, the interaction between the SiNWs and the VOC molecules.

So far, the sensitivity of SiNW FETs functionalized with different silanes has been notoriously low.[30] Improved sensing of nonpolar VOCs and high signal-to-noise ratios have been achieved by controlling the cross-linking bonds between adjacent functional alkyl silane molecules on Si surfaces.[5−7] Sensing nonpolar VOCs has been associated with molecular gating, via two indirect effects: (i) VOC-induced changes in the functional organic layer affect the density of charged monolayer/SiO_2 interface states, causing charged surface states;[5−7] and (ii) changes in the surrounding dielectric medium due to condensation of VOCs on the SiNW surface.[5−7] To gain further understanding of the sensing mechanism of the SiNW-based sensors, we have recently modified SiNW FETs with molecular layers having the same chain length but different end groups.[8] Threshold voltage shifts (ΔV_{th}) and mobility changes ($\Delta\mu_h$) under VOC exposure were recorded.[8] Modeling of the results identified three mechanisms that contribute to the interaction between the functional layers and the VOC molecules:[8] (i) dipole–dipole interaction between the functional surface molecules and polar VOCs; (ii) induced dipole–dipole interaction between the functional surface molecules and nonpolar VOCs; (iii) tilting of the functional surface molecules due to diffusion of VOC molecules. Consequently, the electron-donating/withdrawing properties of the functional molecules' end groups control the

Received: April 7, 2013
Accepted: May 31, 2013
Published: June 3, 2013

dipole orientation of the adsorbed VOC molecules, and, hence, the direction of the threshold voltage shifts. The mobility response was found to be affected mainly due to the diffusion of VOC molecules into the molecular layer that is determined by the functional molecules' end groups.

In the present work, we provided further insight into the sensing mechanism of the molecularly modified SiNW FETs to polar and nonpolar VOCs. SiNW FETs were modified with different functional surface molecules having the same end group and amide bridge bond, but different chain lengths (see Scheme 1). The responses in terms of threshold voltage shifts (ΔV_{th}) and mobility changes ($\Delta \mu_h$) to polar and nonpolar VOCs at different concentrations were studied. A dipole sensing model was used to predict the interaction between the functional molecular layer and the adsorbed VOC molecules on the SiNW surface.

Scheme 1. Schematic Illustration of Different Types of Molecular Surface Functionalization

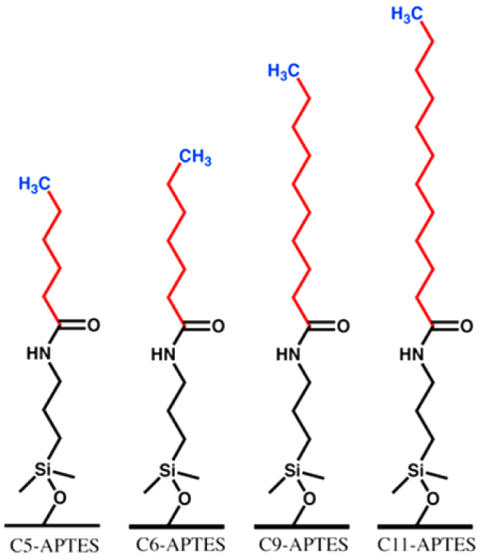

EXPERIMENTAL SECTION

SiNW Synthesis. SiNWs (p-type; length, 8.5 ± 1.5 μm; diameter, 40 ± 8 nm) have been deposited on Si wafers by means of chemical vapor deposition (precursor, 1:20000 gas mixture of SiH_4 and B_2H_6; catalyst, Au), as described in refs 8 and 46. The as-deposited SiNWs had a single-crystalline Si core covered by 5 ± 1 nm of native oxide.

SiNW Array Fabrication. The fabrication process was described in ref 8. Briefly, Au catalyst, native oxide, and residual Au contamination of the SiNW surface were carefully removed by the following treatment: 15 s of buffered HF followed by 2 min of KI:I_2:H_2O (mass ratio 4:1:40). The SiNWs were then dispersed in ethanol by 6 s of ultrasonication (length distribution after sonication: 4−10 μm). SiNWs were spray-coated from solution on precleaned SiOx/Si(100) (p-type; resistivity, 0.001 Ω cm; 300 nm thermal oxide; 10 nmTi/200 nmAu back gate). The spray coating (described in ref 47) generates well-aligned NW arrays (~1 NW/100 μm^2).

SiNW FET Fabrication. After cleaning the substrate with the SiNW array (rinsing with acetone, methanol, and ethanol; 1 min 50 W oxygen plasma; 5s buffered HF), the top source (S)−drain (D) electrodes were deposited (photolithography and lift-off; Karl Suss MA6Mask Aligner) on top of the SiNWs (18 pairs of 10 nmTi/110 nmAu interdigitated electrodes; length, 1300 μm; width, 2 μm; spacing, 2 μm), as described in ref 8. Optical microscopy (Olympus BX51RF-5; dark field mode) and scanning electron microscopy (e-LiNE, Raith, Dortmund, Germany) were used to determine the number of contacted SiNWs.

Molecular Engineering of the SiNW FETs. After surface activation by 60 s of O_x plasma treatment, the devices were processed as follows (described in ref 8): (i) 1 h of immersion in 3-aminopropyltriethoxylsilane (APTES)/dehydrated ethanol (10 mM, 20 mL) at room temperature; (ii) rinsing in acetone, ethanol, and isopropanol and drying by N_2 flow; (iii) 17 h of immersion in acyl chloride solution (10 mM) in chloroform with 10 μL of triethylamine. In this study, we used the acyl chlorides hexanoyl chloride ($C_6H_{11}ClO$), heptanoyl chloride ($C_7H_{13}ClO$), decanoyl chloride ($C_{10}H_{19}ClO$), and dodecanoyl chloride ($C_{12}H_{23}ClO$), which have a common methyl functional group, but differ with their alkyl chain length. Scheme 1 shows the resulting functional layers: C_5-APTES, C_6-APTES, C_9-APTES, and C_{11}-APTES, respectively.

Characterization of the Molecular Layers. X-ray photoelectron spectroscopy (XPS; Thermo VG Scientific, Sigma Probe, England; monochromatized X-ray Al Kα 1486.6 eV source) was used for surface characterization, as described in ref 8. Briefly, dense SiNW layers were spray-coated onto 200 nm Al/Si(100) substrates and molecularly functionalized as described above. Peak fitting software (XPSPEAK version 4.1) was used to analyze the XPS spectra after subtraction of a Shirley background; reference for binding energy calibration: C 1s (C−C) peak at 285.0 eV.

Kelvin probe measurements were used to determine the work function (Φ) of bare and molecularly modified SiNW layers (Farady caged Kelvin Probe system; KP Technology Ltd., UK; N_2 atmosphere; resolution 1−3 mV). InGa was applied for Ohmic connection between the samples' Al back contacts with the Al sample stage. Three repetitions were performed and the results were averaged.

The thickness of each molecular layer was determined by spectroscopic ellipsometer (SE, M-2000 V, J. A. Woollam Co., Inc.) at five incidence angles (60°, 65°, 70°, 75°, and 80°) on an open sample stage, as described in ref 8. For this purpose we deposited the molecular layers on planar Si(111) substrates with 1.7 ± 0.3 nm native oxide, using the same method as for the SiNWs. The functional layer thickness was determined by applying a three-phase functional layer/native oxide/Si(111) model. An absorption-free Cauchy dispersion of the refractive index with values of n (1.46 at 1000 nm, 1.61 at 250 nm) was assumed for all molecular cap-layers. Chem3D software was used to calculate the theoretical molecular modification length.

VOC-Sensing Experiments. The sensing experiments were described in general in ref 8. Briefly, molecularly engineered SiNW FETs with different alkyl chain lengths (C_5-APTES, C_6-APTES, C_9-APTES, and C_{11}-APTES) were mounted onto separate TO_5 holders

Table 1. Properties of the VOCs[48]

VOC	formula	boiling point (°C)	p_o (kPa)[(a)]	K_v	dipole moment (Debye)	density (g cm^{-3})
n-hexane	$CH_3(CH_2)_4CH_3$	68.72	17.60	1.89	0	0.655
n-octane	$CH_3(CH_2)_6CH_3$	125.62	1.47	1.94	0	0.703
n-decane	$CH_3(CH_2)_8CH_3$	171.4	1.58	1.98	0	0.730
ethanol	CH_3CH_2OH	78.24	5.95	24.3	1.69	0.789
1-hexanol	$CH_3(CH_2)_5OH$	156.9	0.95	13.03	1.65	0.814
1-octanol	$CH_3(CH_2)_7OH$	194.7	0.11	10.3	1.76	0.824
1-decanol	$CH_3(CH_2)_9OH$	229	0.015	7.93	1.68	0.830

dx.doi.org/10.1021/am401265z | ACS Appl. Mater. Interfaces 2013, 5, 5748−5756

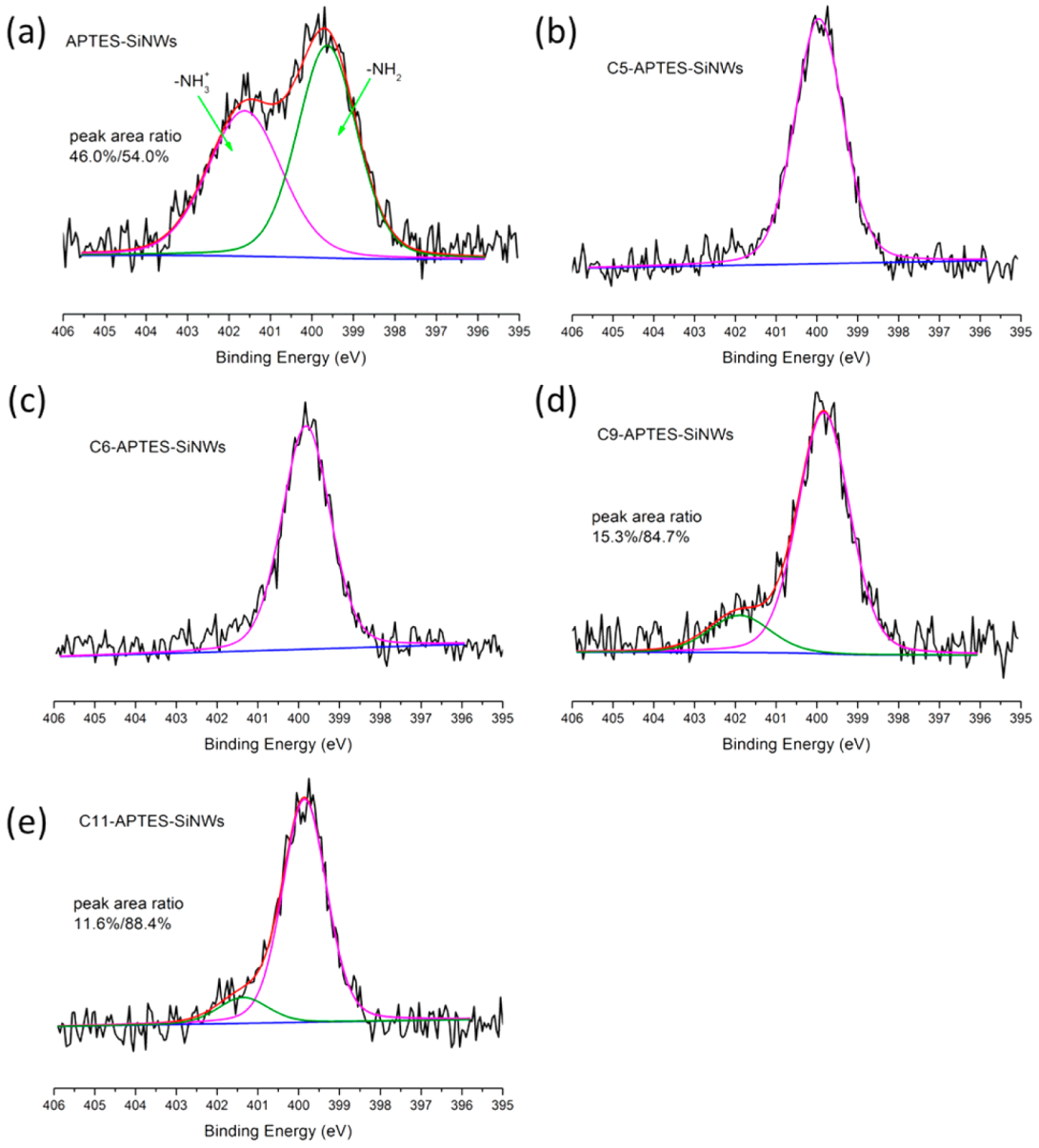

Figure 1. XPS N1s spectra of (a) APTES-SiNWs; (b) C_5-APTES-SiNWs; (c) C_6-APTES-SiNWs; (d) C_9-APTES-SiNWs; and (e) C_{11}-APTES-SiNWs.

by wire-bonding. According to their surface modification, the FET sensors were named as C_5−SiNW FET, C_6−SiNW FET, C_9−SiNW FET, C_{11}−SiNW FET, respectively. The SiNW FET were mounted onto a circuit board in a stainless steel test chamber (volume, 170 cm^3). A Keithley 2636A system SourceMeter and a Keithley 3706 system Switch/Multimeter were used for I_{ds} versus V_g measurements (back sweep from +40 V to −40 V; step, 200 mV; V_{ds}, 2 V) before, during and after exposure to the polar and nonpolar VOCs listed in Table 1. VOC vapors were produced as described in ref 8, using a bubbler system. Purified dry air (8−10% relative humidity) served as reference and as a carrier gas for the VOCs. The vapors were supplied with real-world confounding background humidity at different levels. The responses to the separate VOCs were determined by exposure to VOC vapors at a flow of 5 L/min constant. Signals were collected for 30 min under air flow, followed by 30 min VOC vapor flow (4 cycles with 4 successively increasing concentrations, from p_a/p_o = 0.01−0.08; p_a, VOC's partial pressure; p_o, vapor pressure at room temperature).

RESULTS

Surface Analysis of Molecularly Modified Si NWs. XPS analysis was carried out to determine the surface differences of applied molecular layers. Figure 1 presents the N 1s high-resolution XPS spectra of APTES-SiNWs and C_x-APTES-SiNWs samples. The APTES N1s spectrum stems from: (i) neutral nitrogen (399.3 eV; 47.6% peak area ratio) and (ii) $-NH_3^+$ ions (401.3 eV; 52.4% peak area ratio). In the latter case, hydrogen was transferred from hydroxyl (−OH) groups at the surface to some of the APTES amino groups ($-NH_2$).[49] The N 1s peak was blue-shifted by ∼0.4 eV after the amidation. The part of the N1 peak that stems from positively charged nitrogen could be useful for monitoring the ration of amide reaction, because of the connection with the amino groups of the functional molecules. The $-NH_3^+$ contribution to the N1 peak was not observed for C_5-APTES and C_6-APTES, indicating that the second layer coverage was high. However, for C_9-APTES and C_{11}-APTES, $-NH_3^+$ contributed about

15.3% and 11.6% to the total N1s peak, respectively, implying the relatively low second layer coverage. This can be understood in terms of the steric effect of a relatively larger volume of long chain acyl chloride.

Table 2 lists the thickness of the molecular layers that were deposited on the planar (native) SiO_2/Si (111) substrates that were measured by SE. The experimental results were in good agreement with the theoretically calculated monolayer thickness. The small standard deviations of the experimental data indicated that the molecular modifications were quite homogeneous. As the chain length increases, the difference between the measured thickness and calculated thickness increases. Because each tested molecular layer has the same APTES first layer, the difference in the measured thickness for the long chain molecular layer may come from the lower second acyl chloride coverage of modified molecules.

Table 2. Experimentally Determined Thickness of the Molecular Layers and Theoretically Calculated Monolayer Thickness

	thickness of molecular layer (Å)			
	C_5-APTES	C_6-APTES	C_9-APTES	C_{11}-APTES
measured	12.7 ± 0.4	12.9 ± 0.5	14.5 ± 1.1	15.0 ± 0.5
calculated	13.8	14.8	18.6	21.0

Sensing Characterization of SiNW FETs. In this paper, voltage threshold (V_{th}) and hole mobility (μ_h), extrapolated from the linear part of the $I_{ds}-V_g$ curves, were used to evaluate the sensors' response to various VOCs. Figure 2 shows the response of the C_6−SiNW FET upon exposure to octanol at different concentrations, as a representative example for sensor response. Figure 2a shows that exposing the C_6−SiNW FET to octanol leads to a shift in V_{th} to more negative voltages, and the changes in V_{th}, as compared to dry air, increased as octanol concentration increased. The V_{th} response of the C_6−SiNW FET was rapid, fully reversible, and sensitive to a wide concentration range. Despite the slight increase in the baseline, the response of μ_h in the C_6−SiNW FET to VOC concentration was also rapid .

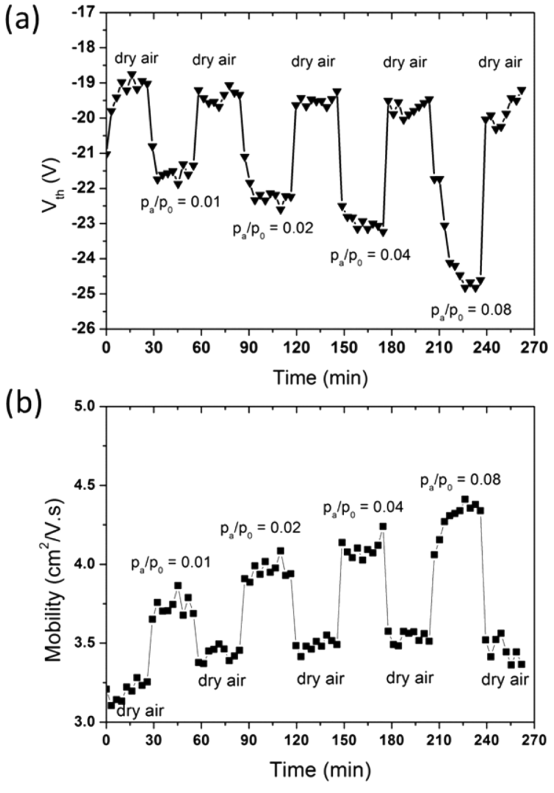

Figure 2. Time-dependent response of C_6-APTES SiNW FET to different concentrations of octanol, as expressed by: (a) V_{th}; and (b) average hole mobility per nanowire.

Sensors Responses in Threshold Voltage Shifts. On the basis of V_{th}−time plots, we calculated ΔV_{th}, which is given by

$$\Delta V_{th} = V_{th-e} - V_{th-a} \quad (1)$$

where $V_{th\text{-}e}$ is the mean value of V_{th} during VOC exposure, and $V_{th\text{-}a}$ is the mean value of V_{th} in dry air, respectively. All sensors showed negative response to the tested VOCs at all applied concentrations (see Figure 3). For nonpolar VOCs at p_a/p_o = 0.01, sensors showed selective sensitivity features. In particular, exposing C_6−SiNW FET to hexane caused the largest ΔV_{th} (−3.97 ± 0.71 V); exposing C_{11}−SiNW FET to octane caused the largest ΔV_{th} (−4.85 ± 0.78 V) but the same sensor showed a weak response to hexane (−2.04 ± 0.46 V) and no response to decane. Exposing C_9−SiNW FET to decane led to the largest ΔV_{th} (−3.49 ± 0.40 V), but no measurable response to hexane or octane.

As the nonpolar VOCs concentration increased from p_a/p_o = 0.01 to 0.08, ΔV_{th} of C_5−SiNW FET upon exposure to hexane and octane increased from −1.41 ± 0.36 V to −2.47 ± 0.20 V, and from 0.69 ± 0.43−0.69 ± 0.43 V to −2.70 ± 0.27 V, respectively. However, the ΔV_{th} of C_5−SiNW FET on exposure to decane decreased from −1.62 ± 0.28 V to −0.99 ± 0.29 V. C_6−SiNW FET showed the largest response at p_a/p_o = 0.01 because of the baseline drift of the sensor. The ΔV_{th} of C_9−SiNW FET and C_{11}−SiNW FET increased with VOC concentration for all nonpolar VOCs.

For polar VOCs, the ΔV_{th} responses of all applied sensors showed VOC concentration dependent character. That is, the higher the VOC concentration, the higher the ΔV_{th}. At $p_a/p_o \geq$ 0.04, it was found that the longer the end alkyl chain length of the molecular layer (afterward in this document, L_{ML}), the higher the ΔV_{th} when sensors are exposed to a given polar VOC at certain concentrations. On the other hand, the ΔV_{th} of a given sensor on exposure to different polar VOCs showed a decreasing trend as VOC chain length increased, except for C_{11}−SiNW FET, which showed the highest response to octanol. Compared to nonpolar VOCs, the sensor response to polar VOCs is higher than the nonpolar counterpart that has the same carbon chain length.

Response of the Hole Mobility of SiNW FETs upon Exposure to VOCs. The hole mobility-based response, was calculated as

$$\Delta\mu_h/\mu_{h-a} = \frac{\mu_{h-e} - \mu_{h-a}}{\mu_{h-a}} \times 100\% \quad (2)$$

where $\mu_{h\text{-}e}$ is the mean value of μ_h at a given VOC exposure step and $\mu_{h\text{-}a}$ is the mean value of μ_h in air. As shown in Figure 4, despite the no response cases, all the rest showed a positive responses at all applied VOC concentrations. At p_a/p_o = 0.01, among the test sensors, C_6−SiNW FET always led to the strongest response on exposure to nonpolar VOCs. As nonpolar VOCs' concentration increased from p_a/p_o = 0.01

dx.doi.org/10.1021/am401265z | ACS Appl. Mater. Interfaces 2013, 5, 5748−5756

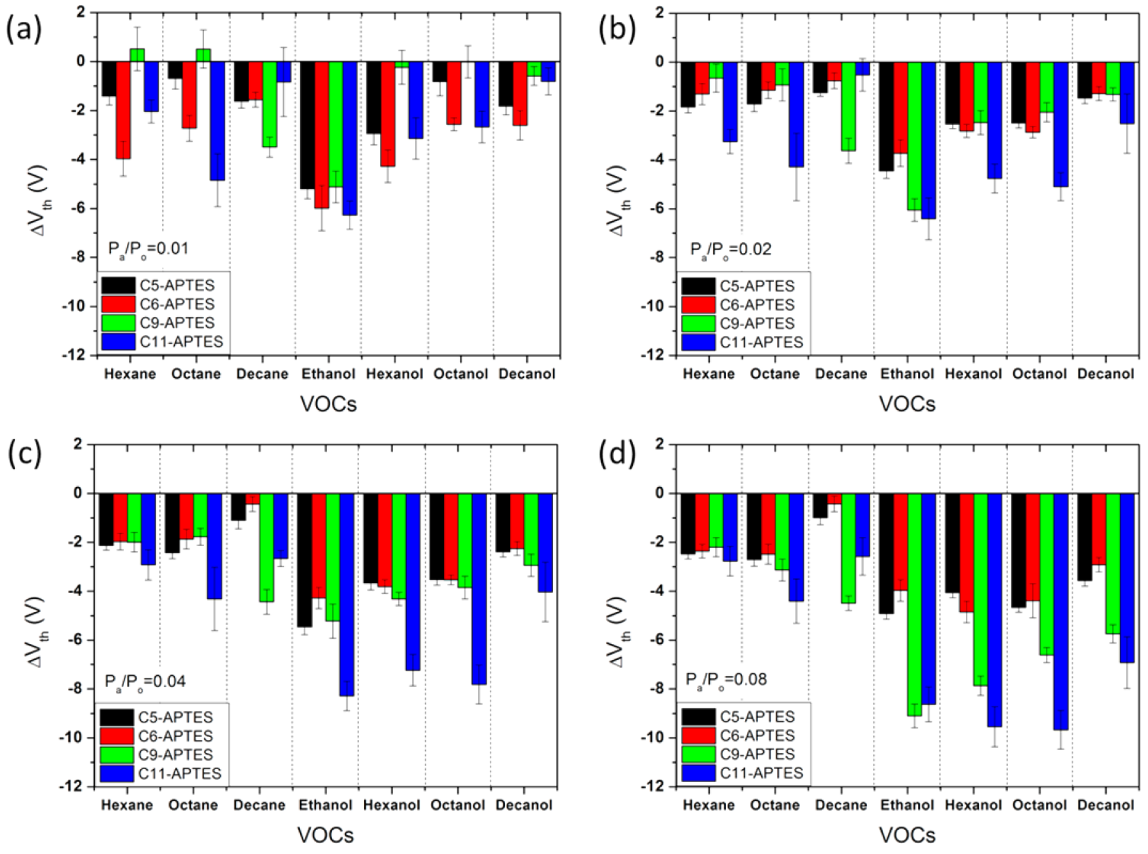

Figure 3. ΔV_{th} of SiNW FET sensors on exposure to nonpolar alkyls and polar alcohols at: (a) p_a/p_o = 0.01; (b) p_a/p_o = 0.02; (c) p_a/p_o = 0.04; and (d) p_a/p_o = 0.08.

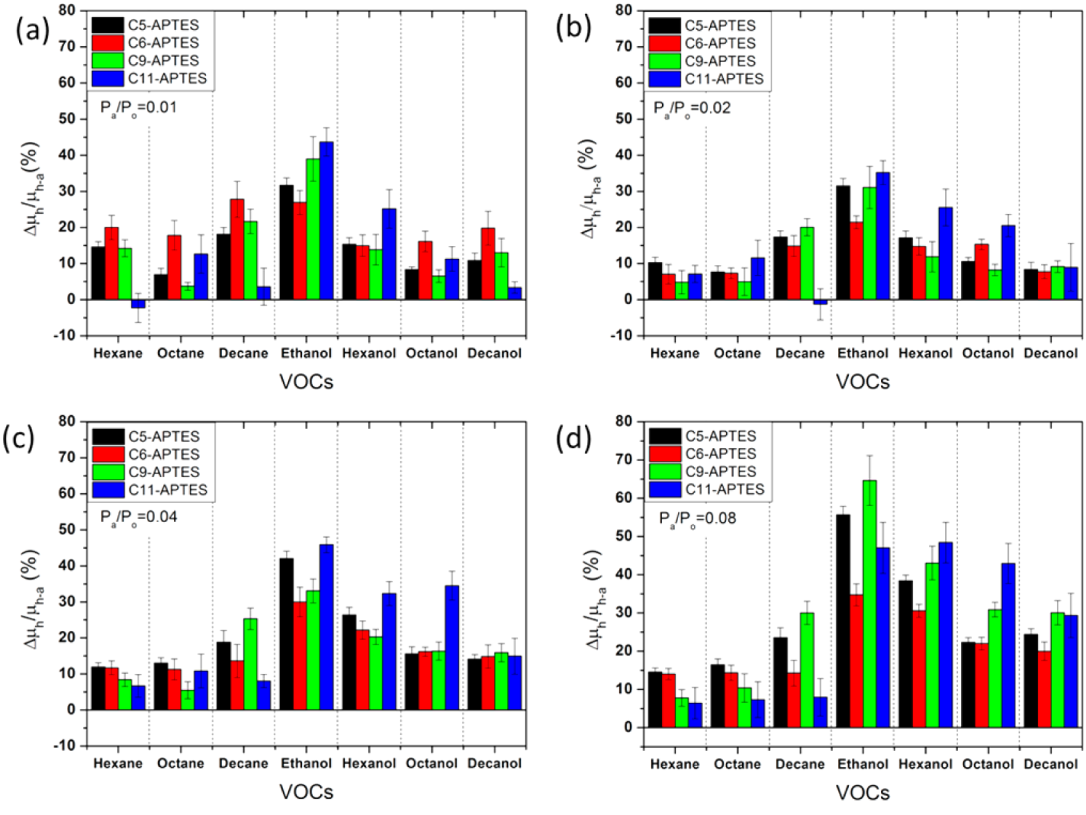

Figure 4. Hole mobility response ($\Delta\mu_h/\mu_{h\text{-}a}$) of SiNW FETs sensors on exposure to nonpolar alkyls and polar alcohols at: (a) p_a/p_o = 0.01; (b) p_a/p_o = 0.02; (c) p_a/p_o = 0.04; and (d) p_a/p_o = 0.08.

dx.doi.org/10.1021/am401265z | ACS Appl. Mater. Interfaces 2013, 5, 5748−5756

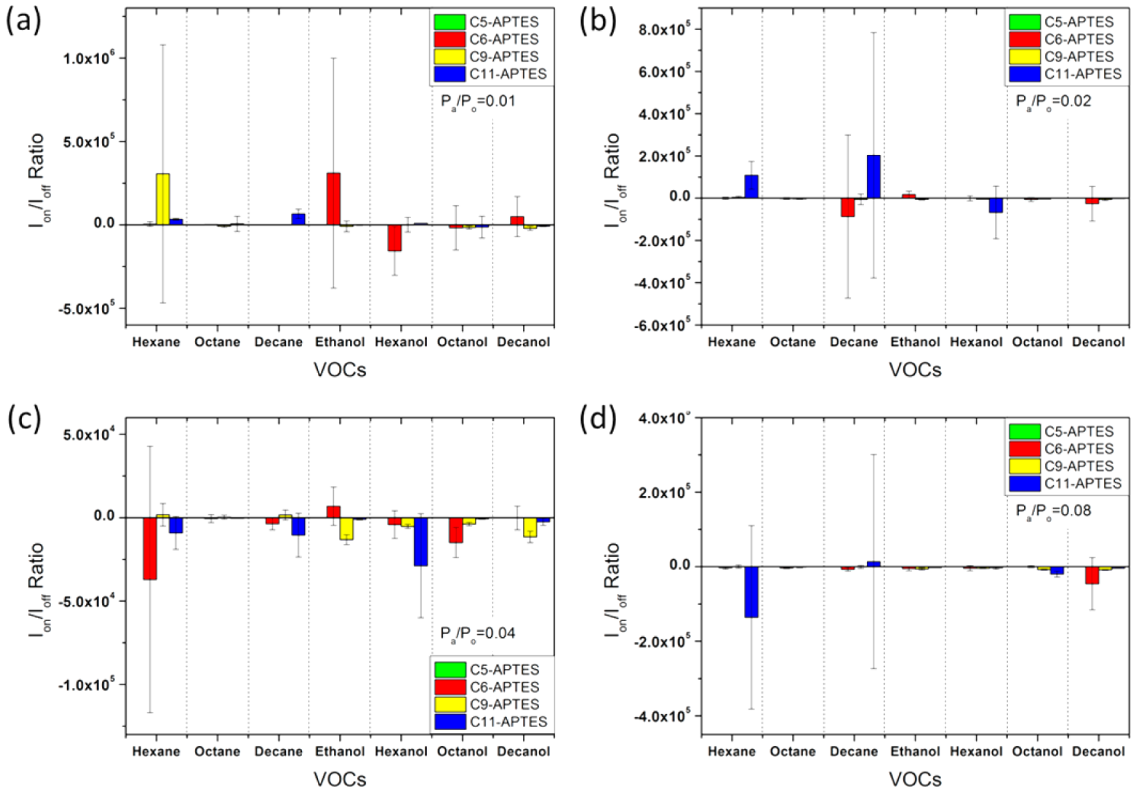

Figure 5. Changes in I_{on}/I_{off} ratio of SiNW FETs sensors on exposure to nonpolar alkyls and polar alcohols at: (a) $p_a/p_o = 0.01$; (b) $p_a/p_o = 0.02$; (c) $p_a/p_o = 0.04$; and (d) $p_a/p_o = 0.08$.

to $p_a/p_o = 0.02$, all sensor responses decreased due to the baseline dramatic drift after the first expose cycle. Then the sensor responses increased with nonpolar VOC concentration. At $p_a/p_o = 0.08$, the longer the nonpolar VOC chain length, the higher the $\Delta\mu_h/\mu_{h\text{-}a}$ response of the C_5−SiNW FET and C_9−SiNW FET. However, the C_6−SiNW FET sensor showed nearly the same response (~14%) when exposed to nonpolar VOCs. In addition, the C_{11}−SiNW FET sensor did not respond to nonpolar VOCs at $p_a/p_o = 0.08$ because of the large standard division of signals.

On exposure to polar VOCs, the sensor responses of all applied sensors increased with increased VOC concentration. The $\Delta\mu_h/\mu_{h\text{-}a}$ of a given sensor on exposure to different polar VOCs showed a trend to decrease as VOC chain length increased. In addition, exposing a sensor with a specific functionalization and to a specific VOC concentration resulted in higher $\Delta\mu_h$ for polar VOCs than for nonpolar VOCs. However, it seems that L_{ML} is not dependent on the sensor response of $\Delta\mu_h/\mu_{h\text{-}a}$. In addition, the sensors' response to polar VOCs was generally higher than to nonpolar ones with the same carbon chain length.

Changes in I_{on}/I_{off} Ratio of SiNW FETs upon VOC Exposure. The changes in I_{on}/I_{off} (i.e., $\Delta(I_{on}/I_{off})$) of SiNW FETs when exposed to VOCs are shown in Figure 5. However, it was difficult to evaluate the changes because of the large deviation of signals. Therefore, $\Delta(I_{on}/I_{off})$ was not useful for evaluating the sensitivity of sensors in the current study.

DISCUSSION

Molecular Layer−SiNW Interaction. The adsorption of polar molecular layers on metal/semiconductor surfaces can produce a substantial shift in the work function. The molecular layer induced work function changes can be expressed as[50]

$$\Delta\Phi = \frac{N\mu_{ML}\cos\theta}{\varepsilon_0\varepsilon_{ML}} \quad (3)$$

N is the packing density of the molecular layer; ε_{ML} is the layer's relative permittivity; ε_0 is the permittivity of free space; θ is the average molecule tilt with respect to the surface normal; μ_{ML} is the dipole moment induced by the molecular layer (caution: orientation of the dipole moment vector from negative to positive charge; a molecule can be understood as a negative dipole if its negative pole is closer to the substrate than its positive pole).

The changes of work function ($\Delta\Phi$), namely the work function of the molecularly modified SiNWs as compared to work function of the bare SiNWs, were evaluated by Kelvin Probe and the results are listed in Table 3. All molecularly modified SiNW layers had negative $\Delta\Phi$ values, suggesting that chemical adsorption of the test molecular layers decreased the work function of SiNWs. All molecular layers had negative dipole moments ($\mu_{ML} < 0$, cf. Equation 3).

VOC-Molecular Layer Interaction. When sensors are exposed to VOCs, the functional molecular layer of the SiNWs

Table 3. Change of the SiNW Work Function ($\Delta\Phi$) after Molecular Engineering

molecular modification	$\Delta\Phi$ (meV)
C_5-APTES	−64.1 ± 15.0
C_6-APTES	−122.8 ± 20.8
C_9-APTES	−100.3 ± 18.3
C_{11}-APTES	−171.3 ± 18.9

dx.doi.org/10.1021/am401265z | ACS Appl. Mater. Interfaces 2013, 5, 5748−5756

can absorb the VOC molecules, which then diffuse from the surface in between the molecule chains. In our recently published paper,[8] we found the V_{th} response of sensors was dominated by the change of dipole moment of molecular layer on exposure to VOCs. The VOC adsorption induced V_{th} shift of SiNW FET can be expressed as[8]

$$\Delta V_{th} = \frac{N}{dC_{BOX}}(\mu'_{ML}\cos\theta' - \mu_{ML}\cos\theta) \quad (4)$$

where d is the thickness of the molecular layer, C_{BOX} is the capacitance of back gate oxide, μ'_{ML} is the molecular layer's dipole moment when exposing the device to a VOC, and θ' is the molecules' average tilt angle under VOC exposure.

The orientation of adsorbed VOCs on the sensor surface is determined by the electronegativity of the molecules' end group. Since the CH_3 end groups of the applied molecular layers tend to donate electrons, the negative pole of the VOC molecules attaches to the surface of the molecular layer. In this condition, the VOC molecule's dipole moment is oriented into the same direction as the dipole moment of the molecular layer. Hence, the adsorption of VOC molecules increases the molecular layer's dipole moment. Supposing that the functional molecules on the Si surface are not tilted after the adsorption of the VOC molecules, the increase in dipole moment causes a shift in V_{th} according to eq 4. Because the dipole moments of the molecular layers are negative, V_{th} shifts into the direction of negative voltages ($\Delta V_{th} < 0$).

The functional molecules' end groups act as antennas; the changes of dipole moment occur only in the case of VOC adsorbed molecules of the molecular layer. For the region that is not covered, the dipole moment of the molecular layer is constant. Our previous report showed that the V_{th} shift of sensors is dominated by surface adsorption, rather than by the diffusion-induced angle tilt angle of the molecular layer of the molecules that compose the SiNW's molecular layer. To simplify the discussion, the tilt angle was supposed to be kept constant. Let γ denote the VOC surface coverage of the molecular layer and $\Delta\mu_{ML}$ denote the dipole moment changes by VOC adsorption on molecular layer. The eq 4 can be rewritten as

$$\Delta V_{th} = \frac{N\gamma\Delta\mu_{ML}\cos\theta}{dC_{BOX}} \quad (5)$$

The coverage fraction can be expressed by the Langmuir adsorption equation[51]

$$\gamma = \frac{\alpha P}{1 + \alpha P} \quad (6)$$

where P is the partial pressure of VOC, and α is the Langmuir adsorption constant, which increases with increased binding energy of adsorption.

For a given sensor on exposure to a given VOC with various concentrations, the coverage fraction of VOC on the molecular layer surface increases with increased VOC concentration, according to eq 6. Therefore, the ΔV_{th} increase with increased VOC concentration matches our experiment data. For a given sensor on exposure to various VOCs with the same concentration, the ΔV_{th} is controlled by the VOC coverage fraction and the dipole moment changes of the molecular layer that are induced by the VOCs. These changes of the molecular layer are related to both polarity of molecular layer and VOCs. Because the dipole−dipole interaction between the molecular layer and polar VOCs is always stronger than the dipole-induced dipole interaction between the molecular layer and nonpolar VOCs, the polar VOCs adsorption induced dipole moment changes of the molecular layer are always stronger than that of nonpolar VOCs with the same chain length. In addition, the higher the volume of the nonpolar VOC the higher the distortion of the molecular modification and the higher the induced dipole moment. Therefore, it can be expected that the long chain nonpolar VOCs induce larger dipole moment changes of the molecular layer than that induced by shorter chain nonpolar VOCs. On the other hand, the stronger the VOC−molecular layer interaction, the higher the binding energy of adsorption. As a result, the strong VOC−molecular layer interaction always leads to a large Langmuir adsorption constant α. The stronger VOC−molecular layer interaction can generate a higher surface coverage of VOCs and a higher $\Delta\mu_{ML}$, both of them increase ΔV_{th} of sensors on exposure to VOCs.

For sensors that are exposed to a given VOC and concentration, the ΔV_{th} response is controlled by the value of α and $\Delta\mu_{ML}$. Since all tested sensors have the same APTES layer, it is likely that the density of the end $-CH_3$ groups of molecular layers is determined by the amide reaction ratio. The longer the chain of the alkyl chloride the larger the steric effect and, therefore, the lower the density of the end $-CH_3$ groups (Table 2 and Figure 1). In this context, it should be noted that the APTES layer has a negative response to VOCs.[8] Thus, the ΔV_{th} of sensors with longer L_{ML} (C_9-APTES and C_{11}-APTES) can be considered as a combination response of unreacted APTES and C_x-APTES molecules (Scheme 2). In addition, the diffused VOC molecules between molecular layer free spaces can also change the dipole moment of the molecular layer and make a contribution to ΔV_{th}. Because of the longer L_{ML} and lower second layer reaction ratio, the interspace volume of longer chain molecular layer is larger than that of the shorter chain molecular layer. As a result, longer chain molecular layers can adsorb more VOCs than shorter chain molecular layers. The increase of μ_h when SiNW FETs were exposed to VOCs could be attributed to a decrease in the surface states density.[6] The absence of a systematic relationship between the $\Delta\mu_h/\mu_{h\text{-}a}$ and the L_{ML} could be attributed to the weak effect of the alkyl chain length on the VOC diffusion into the molecular layer.

Scheme 2. Schematic Demonstration of SiNW FET Modified with Long Alkyl Chain Molecular Layers upon Exposure to VOCs

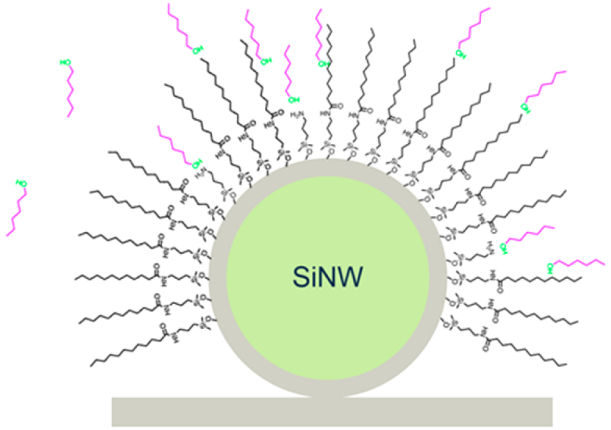

dx.doi.org/10.1021/am401265z | ACS Appl. Mater. Interfaces 2013, 5, 5748−5756

SUMMARY AND CONCLUSIONS

We studied the effect of chain length of molecular layer on the sensing performance of SiNW FETs to polar and to nonpolar VOCs. All molecularly modified SiNW FETs showed negative response in ΔV_{th} and positive response in $\Delta\mu_h/\mu_{h\text{-}a}$ when they were exposed to polar and to nonpolar VOCs. On exposure to a given concentration of VOCs, ΔV_{th} response increased with chain length of the molecular modification. However, there is no dependence of the $\Delta\mu_h/\mu_{h\text{-}a}$ response on the chain length of the molecular layer. Analysis of the responses with an electrostatic-based model suggests that the sensor response in ΔV_{th} is dependent on the VOC concentration, VOC vapor pressure, VOC-molecular layer binding energy, and VOC adsorption induced dipole moment changes of molecular layer. Furthermore, the large intermolecule space of the long chain molecular layer, which is due to the longer chain length of the molecular layer and relative low second layer amide reaction ratio, enable it to adsorb more VOC molecules than the short chain molecular layer, thereby increasing the ΔV_{th} response to VOCs.

AUTHOR INFORMATION

Corresponding Author

*E-mail: hhossam@tx.technion.ac.il.

Notes

The authors declare no competing financial interest.

ACKNOWLEDGMENTS

The research leading to these results has received finding from the FP7-Health Program under the LCAOS (Grant 258868). The authors acknowledge the Israel Council for Higher Education for partial support of Bin Wang's postdoctoral fellowship, Dr. Silke Christiansen (Max-Planck-Institute for the Science of Light, Germany) for providing some of the SiNWs reported in the current study, study and Dr. Ulrike (Mirjam) Tisch (Technion-IIT) for reviewing the manuscript.

REFERENCES

(1) Wallace, L. A. *Annu. Rev. Energy Environ.* **2001**, *26*, 269−301.
(2) Hakim, M.; Broza, Y. Y.; Barash, O.; Peled, N.; Phillips, M.; Amann, A.; Haick, H. *Chem. Rev.* **2012**, *112*, 5949−5966.
(3) Tisch, U.; Haick, H. *Rev. Chem. Eng.* **2010**, *26*, 171−179.
(4) Tisch, U.; Haick, H. *MRS Bull.* **2010**, *35*, 797−803.
(5) Paska, Y.; Haick, H. *ACS Appl. Mater. Interfaces* **2012**, *4*, 2604−2617.
(6) Paska, Y.; Stelzner, T.; Assad, O.; Tisch, U.; Christiansen, S.; Haick, H. *ACS Nano* **2012**, *6*, 335−345.
(7) Paska, Y.; Stelzner, T.; Christiansen, S.; Haick, H. *ACS Nano* **2011**, *5*, 5620−5626.
(8) Wang, B.; Haick, H. *ACS Appl. Mater. Interfaces* **2013**, *5*, 2289−2299.
(9) Zilberman, Y.; Ionescu, R.; Feng, X.; Mullen, K.; Haick, H. *ACS Nano* **2011**, *5*, 6743−6753.
(10) Bachar, N.; Mintz, L.; Zilberman, Y.; Ionescu, R.; Feng, X.; Müllen, K.; Haick, H. *ACS Appl. Mater. Interfaces* **2012**, *4*, 4960−4965.
(11) Zilberman, Y.; Tisch, U.; Shuster, G.; Pisula, W.; Feng, X.; Mullen, K.; Haick, H. *Adv. Mater.* **2010**, *22*, 4317−4320.
(12) Peng, G.; Tisch, U.; Haick, H. *Nano Lett.* **2009**, *9*, 1362−1368.
(13) Peng, G.; Trock, E.; Haick, H. *Nano Lett.* **2008**, *8*, 3631−3635.
(14) Bayn, A.; Feng, X.; Müllen, K.; Haick, H. *ACS Appl. Mater. Interfaces* **2013**, *5*, 3431−3440.
(15) Konvalina, G.; Haick, H. *ACS Appl. Mater. Interfaces* **2012**, *4*, 317−325.
(16) Hakim, M.; Billan, S.; Tisch, U.; Peng, G.; Dvrokind, I.; Marom, O.; Abdah-Bortnyak, R.; Kuten, A.; Haick, H. *Br. J. Cancer* **2011**, *104*, 1649−1655.
(17) Tisch, U.; Billan, S.; Ilouze, M.; Phillips, M.; Peled, N.; Haick, H. *CML−Lung Cancer* **2012**, *5*, 107−117.
(18) Tisch, U.; Aluf, Y.; Ionescu, R.; Nakhleh, M.; Bassal, R.; Axelrod, N.; Robertman, D.; Tessler, Y.; Finberg, J. P. M.; Haick, H. *ACS Chem. Neurosci.* **2011**, *3*, 161−166.
(19) Barash, O.; Peled, N.; Tisch, U.; Bunn, P. A.; Hirsch, F. R.; Haick, H. *Nanomedicine* **2012**, *8*, 580−589.
(20) Barash, O.; Peled, N.; Hirsch, F. R.; Haick, H. *Small* **2009**, *5*, 2618−2624.
(21) Haick, H.; Hakim, M.; Patrascua, M.; Levenberg, C.; Shehada, N.; Nakhoul, F.; Abassi, Z. *ACS Nano* **2009**, *3*, 1258−1266.
(22) Tisch, U.; Schlesinger, I.; Ionescu, R.; Nassar, M.; Axelrod, N.; Robertman, D.; Tessler, Y.; Azar, F.; Marmur, A.; Aharon-Peretz, J.; Haick, H. *Nanomedicine (Future Medicine, London)* **2012**, *8*, 43−56.
(23) Ionescu, R.; Broza, Y.; Shaltieli, H.; Sadeh, D.; Zilberman, Y.; Feng, X.; Glass-Marmor, L.; Lejbkowicz, I.; Mullen, K.; Miller, A.; Haick, H. *ACS Chem. Neurosci.* **2011**, *2*, 687−693.
(24) Engel, Y.; Elnathan, R.; Pevzner, A.; Davidi, G.; Flaxer, E.; Patolsky, F. *Angew. Chem., Int. Ed.* **2010**, *49*, 6830−6835.
(25) Hahm, J.; Lieber, C. M. *Nano Lett.* **2004**, *4*, 51−54.
(26) He, B.; Morrow, T. J.; Keating, C. D. *Curr. Opin. Chem. Biol.* **2008**, *12*, 522−528.
(27) Huang, C.; Katz, H. E.; West, J. E. *Langmuir* **2007**, *23*, 13223−13231.
(28) Li, D.; Song, S.; Fan, C. *Acc. Chem. Res.* **2010**, *43*, 631−641.
(29) Liu, L.; Shao, M.; Lee, S.-T. *J. Nanoeng. Nanomanufact.* **2012**, *2*, 102−111.
(30) McAlpine, M. C.; Ahmad, H.; Wang, D. W.; Heath, J. R. *Nat. Mater.* **2007**, *6*, 379−384.
(31) Patolsky, F.; Zheng, G.; Lieber, C. M. *Nanomedicine* **2006**, *1*, 51−65.
(32) Patolsky, F.; Zheng, G. F.; Lieber, C. M. *Nat. Protoc.* **2006**, *1*, 1711−1724.
(33) Stern, E.; Vacic, A.; Reed, M. A. *IEEE Trans. Electron Devices* **2008**, *55*, 3119−3130.
(34) Wang, W. U.; Chen, C.; Lin, K. H.; Fang, Y.; Lieber, C. M. *Proc. Nat. Acad. Sci.* **2005**, *102*, 3208−3212.
(35) Guo, Q. S.; Kong, T.; Su, R. G.; Zhang, Q.; Cheng, G. S. *Appl. Phys. Lett.* **2012**, *101*, 093704.
(36) Kong, T.; Su, R. G.; Zhang, B. B.; Zhang, Q.; Cheng, G. S. *Biosens. Bioelectron.* **2012**, *34*, 267−272.
(37) Bashouti, M. Y.; Sardashti, K.; Schmitt, S. W.; Pietsch, M.; Ristein, J.; Haick, H.; Christiansen, S. H. *Prog. Surf. Sci.* **2013**, *88*, 39−60.
(38) Assad, O.; Puniredd, S. R.; Stelzner, T.; Christiansen, S.; Haick, H. *J. Am. Chem. Soc.* **2008**, *130*, 17670−17671.
(39) Puniredd, S. R.; Assad, O.; Haick, H. *J. Am. Chem. Soc.* **2008**, *130*, 13727−13734.
(40) Puniredd, S. R.; Assad, O.; Haick, H. *J. Am. Chem. Soc.* **2008**, *130*, 9184−9185.
(41) Puniredd, S. R.; Assad, O.; Stelzner, T.; Christiansen, S.; Haick, H. *Langmuir* **2011**, *27*, 4764−4771.
(42) Bashouti, M. Y.; Tung, R. T.; Haick, H. *Small* **2009**, *5*, 2761−2769.
(43) He, T.; Corley, D. A.; Lu, M.; Di Spigna, N. H.; He, J. L.; Nackashi, D. P.; Franzon, P. D.; Tour, J. M. *J. Am. Chem. Soc.* **2009**, *131*, 10023−10030.
(44) Kornblum, L.; Paska, Y.; Haick, H.; Eizenberg, M. *J. Phys. Chem. C* **2013**, *117*, 233−237.
(45) He, T.; He, J. L.; Lu, M.; Chen, B.; Pang, H.; Reus, W. F.; Nolte, W. M.; Nackashi, D. P.; Franzon, P. D.; Tour, J. M. *J. Am. Chem. Soc.* **2006**, *128*, 14537−14541.
(46) Stelzner, T.; Andra, G.; Wendler, E.; Wesch, W.; Scholz, R.; Gosele, U.; Christiansen, S. *Nanotechnology* **2006**, *17*, 2895−2898.
(47) Assad, O.; Leshansky, A. M.; Wang, B.; Stelzner, T.; Christiansen, S.; Haick, H. *ACS Nano* **2012**, *6*, 4702−4712.

(48) Haynes, W. M. *CRC Handbook of Chemistry and Physics*, 93rd ed. (Internet Version 2013); CRC Press/Taylor and Francis: Boca Raton, FL, 2013.
(49) Wanger, C. D.; Riggs, W. M.; Davis, L. E.; Moulder, J. F.; Muilenberg, G. E. *Handbook of X-Ray Photoelectron Spectroscopy*; Perkin-Elmer Corp.: Eden Prairie, MN, 1979.
(50) Moench, W. *Semiconductor Surfaces and Interfaces*, 3rd ed.; Springer-Verlag: Berlin, Germany, 2001.
(51) Masel, R. I. *Principles of Adsorption and Reaction on Solid Surfaces*; Wiley-Interscience: New York, 1996.